A novel way of using reverberation chambers through time reversal

Houmam Moussa, Andrea Cozza, Michel Cauteman

A NOVEL WAY OF USING REVERBERATION CHAMBERS THROUGH TIME-REVERSAL

H. MOUSSA, A. Cozza, M. Cauterman
Département de Recherche en Electromagnétisme
(CNRS, Supelec-Univ. Paris-Sud)
SUPELEC, 3 rue Joliot-Curie, 91192 Gif-sur-Yvette Cedex, France.

ABSTRACT:

In this paper, a novel way of using reverberation chambers (RCs) is proposed. The feasibility of coherent deterministic cylindrical wavefronts generation inside RCs is investigated by applying the time reversal technique on electromagnetic waves. To achieve that, we designed a new radiated-immunity testing tool called a time-reversal electromagnetic chamber (TREC) to generate coherent wavefronts towards equipment-under-test (EUT). High field strength levels are achieved as we focus the energy on a small volume around the EUT. The quality of a cylindrical wavefront converging towards a EUT is evaluated for different configurations of the TREC system.

I. INTRODUCTION

The electromagnetic interference (EMI) shielding is a critical requirement for aerospace structures as the reliance on electronic control systems increases. An important difference compared to ground structures is the weight limitations, which could affect directly the lifetime of a communication satellite extending it by years as few ounces saved could be replaced by extra fuel. According to this, radiated-immunity of carbon composite materials [1], EMI gaskets [2] or even complete aerospace applications must be tested.

Different test methods have been used over the years to verify the shielding effectiveness of equipments. Mainly, two different types of facility, among others, are often used nowadays for high frequency EMC radiated-immunity tests: the anechoic and semi-anechoic chambers [3] and the reverberation chambers (RCs) [4]. Usually, comparisons are done between RCs and ACs [5] each one having their own advantages and disadvantages.

For testing in ACs, the main problem is to assure that the most critical directions and polarizations have been used because their numbers are limited during standard tests. On the other hand, the shape of the waveform is well defined and the levels of the field magnitude are known in a deterministic way.

Otherwise, in RCs all the weaknesses of the EUT are statistically excited at the same time but therefore it is not possible to know which incoming directions and polarizations revealed them. Thus, it is difficult to exploit the test results to improve the EUT shielding effectiveness. Nevertheless, thanks to its resonances properties, RCs allow to generate high-intensity fields with a relatively low-level injected power.

This paper proposes a new way of using RCs for EMC testing with the generation of high-intensity deterministic temporal wavefronts inside them instead of a high-intensity, statistically homogeneous and isotropic field. We took here the advantage of the coherent wavefronts as well as plane-waves in ACs testing, and the high-intensity of the field as in RCs. This may be accomplished using the time-reversal technique [6] on electromagnetic waves inside RCs.

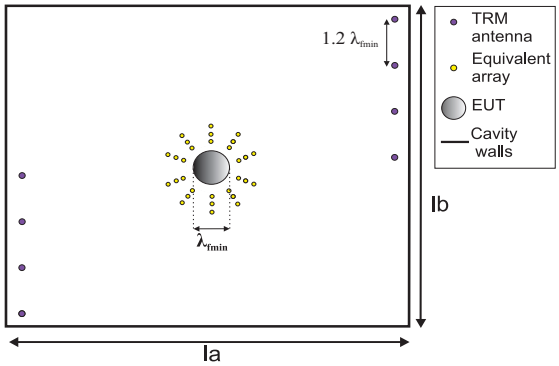

Figure 1. Time-reversal electromagnetic chamber. The TRM antennas are located at least at 0.4 λ_{fmin} from the cavity walls with λ_{fmin} the wavelength corresponding to the minimal frequency of an excitation signal. "la" is the width of the rectangular cavity and "lb" its height.

To validate this property, we simulated the TREC system, presented in the Figure 1, in a simplified 3D configuration as one dimension of the cavity is reduced below the wavelength of use. It provides a realistic test environment for the properties of the time-reversal technique as applied in a highly reverberating cavity, although not as complex as for a fully 3D structure because we are only dealing with a scalar field with just one vertical polarization. This allowed us to study different configurations of the system. In the following section, an introduction to the time reversal technique is given and a new paradigm of its use is proposed in order to apply it to EMC testing. Then an example of a cylindrical wavefront illuminating an EUT is presented. Finally, a study of the quality of the reconstructed wavefront is carried out for different configurations of the TREC system before presenting some perspectives for upcoming works to propose the TREC as a complementary EMC testing tool with respect to RCs and ACs.

II. A NEW PARADIGM FOR TIME REVERSAL

The time reversal is a time-domain technique originally developed in acoustics [6], [7] and more recently in electromagnetism [8], [9] to focus a wave on point-like transceivers. The main idea is to let acoustic or electromagnetic waves back-propagate in a complex environment and focus back onto the initial point of their generation. To achieve that, time reversal requires two steps: first, the field must be sampled in every direction by an antenna array, disposed on an area enclosing the source of the field, called a time-reversal mirror (TRM) [6]. To be precise, the electric field $e(\vec{\rho}_i,t)$ detected by a set of antennas located at positions $\vec{\rho}_i$, is sampled during a time interval ΔT. Then, in a second step, the field is retransmitted by the same antennas in a reversed temporal chronology (last in, first out) equivalent to the transmission of $e(\vec{\rho}_i,\Delta T-t)$. This procedure allows converting a divergent wave issued from an electromagnetic source into a convergent wave focusing on this source.

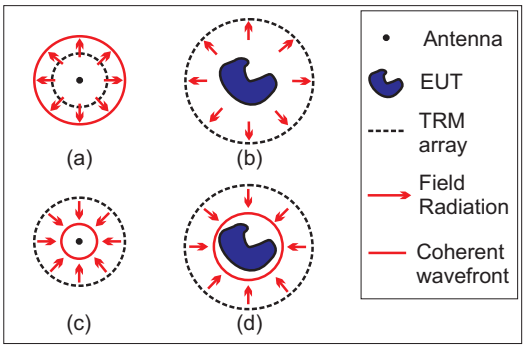

Figure 2. New paradigm for time reversal: (a) and (c) are respectively the first and second step of the time reversal for a point-like antenna; (b) and (d) are the ones for an electrically large EUT.

Also, in [10], it has been proven that in an RC the number of antennas needed for the TRM can be reduced to a single one, taking advantage of the reflections as if the field were sampled in every direction.

Nevertheless, in EMC tests, EUT are electrically large systems that cannot be considered as an antenna with an input port that can be excited. Therefore, if we are interested in generating a particular wavefront during the second step of time reversal, we have to find another way to obtain the appropriate signals to be applied on the TRM elements. If we draw an analogy with a point-like antenna, as shown in the Figure 2, we should define a system that leads to these signals by radiating a pattern in the direction of the TRM as if an antenna instead of the EUT did it.

To carry through this issue, we used the field equivalence principle [11] to define a boundary surface around the EUT on which equivalent electromagnetic currents radiates this pattern. As we are dealing with a transverse propagation of the field in this simplified 3D study this surface became a simple line. Thus, we implement it with an array of isotropic elements called equivalent array in Figure 1.

Unfortunately, isotropic elements radiates both outwards and towards the EUT whereas the radiation pattern must be away from the EUT in order to avoid the reflection of the field on it, especially as it is made out of a piece of metal. Indeed, as the distance between the equivalent array and the EUT is less than $\lambda_{fmin}/3$, the TRM antennas will sample the superposition of the portion of the field radiated in their direction and the reflection of the other one radiated towards the EUT delayed by $2\,\lambda_{fmin}/(3\,c_0)$, with c_0 the wave-propagation speed in the cavity. This will lead to the degradation of the wavefront even before being sampled in the time-reversal first step. Therefore, a solution is to extend the equivalent array with two additional circular arrays of isotropic sources, (cf. Figure 1), in order to generate destructive interferences of the fields towards the EUT and constructive ones away from it. The idea is to space the arrays by a distance of $\lambda_{fc}/4$ (λ_{fc} is the wavelength corresponding to the central frequency of an excitation signal, x(t), on the array) and shift their phases by one radian, i.e., from the closest circular array to the EUT to the further one, phases are respectively 2, 1 and 0 radians. It is the same principle as for end-fire arrays except it is computed to maximize the radiation of the energy outside the equivalent array and minimize it inwards.

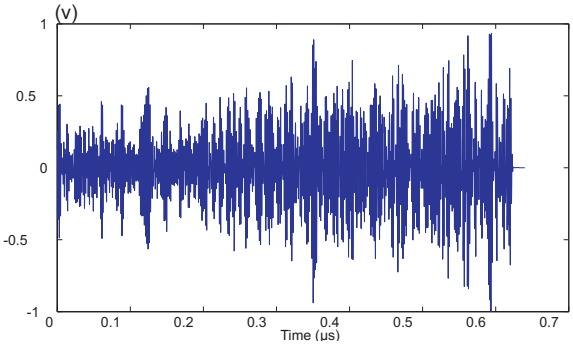

Figure 3. Signal y(t) applied on one TRM antenna.

For instance, when we feed the elements of the equivalent array with x(t), this signal gives rise to a wavefront which propagates inside the cavity and is sampled by the TRM antennas during a period ΔT. Then the signals $y_i(t)$, obtained on each TRM antenna after this period, are time-reversed and emitted again through the TRM. Finally, after the same time length ΔT, we obtain a signal $s_j(t)$ on the equivalent array elements apiece. We must precise that all the energy that is injected in the cavity is contained in the $y_i(t)$ signals and the fact that we are limiting their time length, for computational issues, places us in a worst case compared to experimental setups. Indeed, we can increase tremendously the recording time with real measurements and thus

focusing more and more energy in the impacting wavefront, thanks to the time-reversal technique, in order to attain higher field levels, as the volume of the coherent field is restricted around the EUT instead of being spread in the entire cavity.

We observe in Figure 4 the comparison between the excitation signal reversed in time x(-t) and the signal s(t) on a probe in the center of the equivalent array without the EUT for the case of a single range array and a three phased ranges. We can see that the signal $s_2(t)$, obtained by the use of a non directive equivalent array, shows a distortion in his shape compared to the initial pulse x(t) while it is not the case for the reconstructed signal $s_1(t)$ from the use of a directive array. Also, we notice negligible oscillations on the sides of the reconstructed signals that are not present in x(t). We should remind that the resonant modes of the cavity are the basis functions that allow establishing the field in the cavity and each mode excited contributes to the reconstruction of any radiation pattern inside it. Therefore, as this basis is not complete, the reconstruction of the signal will be affected by these oscillations. This is the same as for the Gibbs phenomenon for a square wave when the number of terms of its Fourier series expansion is truncated leading to ringing artifacts. In this case, these artifacts are residual errors of the reconstructed signals and can be considered as a "noise" with respect to the initial pulse shape.

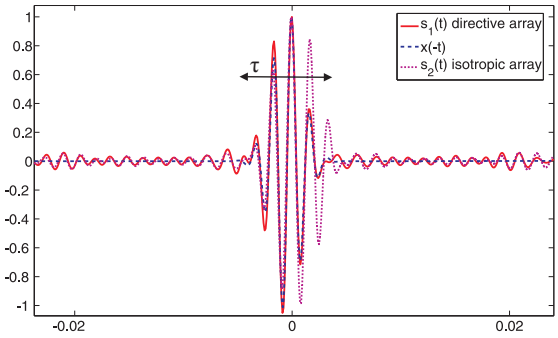

Figure 4. Temporal-reconstructed signals on a probe in the center of the equivalent array. x(t) is a pulse modulated excitation signal. $s_1(t)$ is the reconstruction of x(t) with a three phased ranges array while $s_2(t)$ is the one with a single range. The signals are normalized to their respective maxima and τ is the length of x(t).

The RC establishes a propagation channel between the equivalent array and the antennas of the TRM. As a matter of fact, its resonant modes allow the transmission of energy inside the TREC system so the frequency and the bandwidth of an excitation signal x(t) must be set to excite an important number of modes in order to reduce the ringing artifacts.

Thus, we decide to feed the system with a Gaussian-modulated pulse with a central frequency chosen by the use of the Weyl's formula [12], which estimates the modal density n_0 associated to a given frequency and fixed dimensions of the cavity. According to the height l_b of the rectangular cavity, we fixed the spatial length of the pulse $\Delta s = l_b/4$ to be able to observe the propagation of the wavefront generated by the equivalent array before any reflection on the cavity walls. Therefore, as we are dealing with a Gaussian signal, we can link its time length Δt with the bandwidth of its spectrum $\Delta\omega$ if we define these quantities relatively to the 3 dB amplitude attenuation as follow: $\Delta\omega = 12\ln(2)/\pi\Delta t$. Finally, as $\Delta s = c_0\Delta t$ we can set the bandwidth of x(t) defined as: $\Delta\omega = 48\ln(2)c_0/\pi l_b$.

Moreover, we can assume that during a certain temporal window, before any interaction between the wavefront and the walls, the propagation happens in the same conditions as in free space. Therefore, we are able to use free-space synthesis rules and design the equivalent array for radiating given time waveform. Afterwards, the properties of the time-reversal technique will reproduce backwards this temporal window after a transient period of incoherent field corresponding to the interferences of the multiple reflections of the wavefront inside the TREC. We can remark that this incoherent field has similar statistical properties to the ones classically generated in RCs. In this study, we designed a cylindrical wavefront for the sake of simplicity so all the elements of the equivalent array are fed with the same signal x(t) whereas whenever a phase is added between the isotropic elements we are able to create directive wavefronts [13].

We can notice that the TREC system allows now to obtain the first-step time-reversal TRM signals by the generation of the equivalent-array field radiation with the EUT already present inside it. Therefore, all the interactions between the emitted pulse x(t) and the EUT during the sampling of the field by the TRM antennas are taken into account directly in the antenna signals. In contrast, for the classical use of RCs, it is hard if not impossible, to predict the effect of the EUT on the propagation medium when it is introduced in the facility without performing again the calibration of the chamber.

III. NUMERICAL RESULTS

In order to validate the generation of coherent wavefronts inside an RC, we carried out numerical simulations of the TREC system under a full-wave electromagnetic transient solver using the finite integration technique as implemented in the software CST's Microwave Studio.

The cavity modeled (cf. Figure 1) has the following electrical dimensions: l_a=16 λ_{fc}, l_b=13.2 λ_{fc} and l_c=0.6 λ_{fc}. The EUT is modeled by a cylindrical shape made out of a perfect conductor with a diameter of λ_{fc} and a thickness of λ_{fc} /2. For the excitation signal x(t), we used a pulse-modulated signal with a central frequency of 600 MHz and a bandwidth of 500 MHz which leads to a theoretical modal density of 5.25 modes/MHz estimated by Weyl's formula with respect to the cavity dimensions. The length of the simulation ΔT = 0.63 µs, limited by computational-time reasons.

The TRM is composed of 8 dipoles of a length of λ_{fc} /2 placed inside the cavity as shown in Figure 1. Attention has been paid to put the antennas at, at least, 0.3 λ_{fmin} from the cavity walls. Contrary to the equivalent array elements positions, the TRM antennas must be placed sufficiently far from each other in order to record uncorrelated signals, thus giving complementary samples of the field.

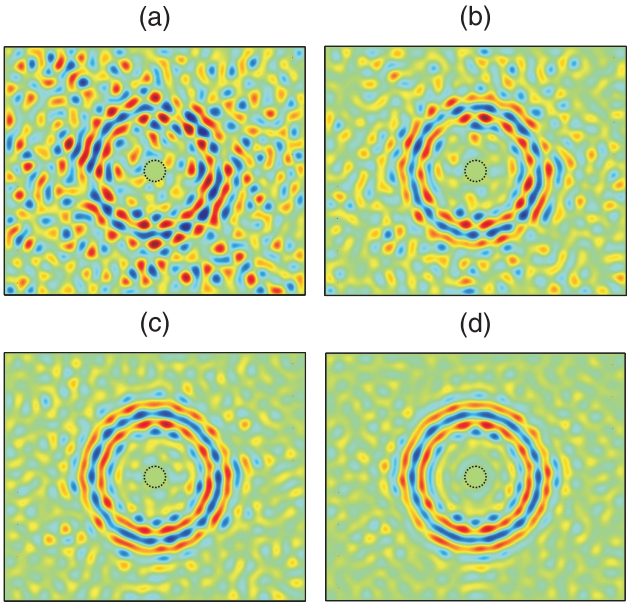

Figure 5. Reconstructed cylindrical wavefront during the second step of the time reversal: (a) 2 antennas used for the TRM; (b) 4 antennas used for the TRM; (c) 6 antennas used for the TRM; (d) 8 antennas used for the TRM. The dash line represents the EUT.

About the equivalent array present in the Figure 1, we placed 3 circular arrays of 32 ideal probes around the EUT to prevent coupling between its elements since ideal probes measure directly the field without providing any modification of the propagation medium. As the TREC is a reciprocal system, we inject the excitation signal directly on the TRM antennas, one by one, and collect the signals on the probes rather than the opposite because the simulator does not allow exciting probes. Then, thanks to the linearity of the system, we reverse in time and sum the signals by post-processing to obtain the right signal to be applied on each TRM antenna for the second step of the time reversal.

Based on the same principle, we define a set of 2D E-field monitors at different instants for the simulations of the time-reversal second step applied to each TRM antenna alone and sum the results by post-processing. By doing that, we are able to study the influence of the number of active TRM antennas and their locations for 255 possible combinations of the different numbers of active antennas used among the 8 ones, presented in Section V. For instance, numerical results of a cylindrical wavefront converging towards a EUT are shown in the Figure 5. We can observe that the quality of the reconstructed wavefront is dependent on the number of antennas used simultaneously for the TRM. As the number increases, so does the contrast between the coherent part of the field and the background in term of magnitude level. If the reconstruction was perfect, the value of the field in the background would be null and the fact that it is not the case is due to the filter of the excitation pulse continuous spectrum by the cavity discrete resonant modes. In fact, the cavity dimensions and the frequency of the excitation signal limit the number of available modes. Moreover, the number of excited modes will be dependent on the number of antennas and their positions used to feed the cavity and thus defines an "effective modal density" that could be at most equal to the estimated modal density n_0 if all available modes are excited.

IV. QUALITY OF THE RECONSTRUCTED WAVEFRONT

We are interested in verifying the quality of the reconstructed cylindrical wavefront, to that aim: we analyze the values of the field over a circle placed on the phase center of the wavefront and with a radius covering one of its arcs. We visualized the magnitudes of the field versus the angle in the graph presented in Figure 6 for the circle covering the central lobe of the wavefront just before impacting on the EUT.

We defined a signal to noise ratio (SNR) between μ^2, the square average of the field values on the

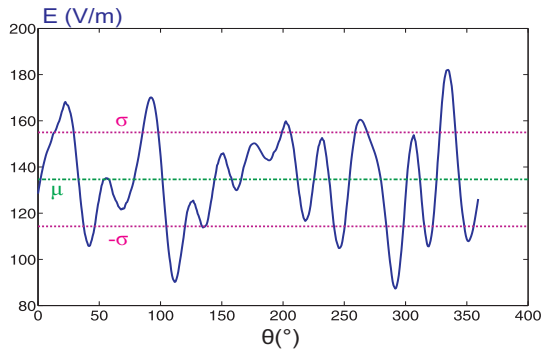

Figure 6. E-filed magnitudes over the angles of one arc. µ is the mean value (136 V/m) of E and σ its rms standard deviation (19 V/m) while 1V peak signal is applied on the TRM antennas.

previously introduced circle, and the square of the average of the incoherent background field, considered as a "spatial noise" with respect to the deterministic wavefront. Most importantly, we have verified that, σ; the root-mean-square (rms) standard deviation from the mean of the wavefront field magnitudes has the same level than the background field average level during the focusing of the waveform. Ideally, a perfect cylindrical wavefront in free space would have a constant value on one of its arcs and a null rms standard deviation so the fluctuations seen in Figure 6 can directly be attributed to the addition of the background incoherent field. We should remark that as we are dealing here with a converging wavefront, during its propagation towards the EUT, its surface decreased in size while the magnitude of the field increased to respect the conservation of the energy density on the wavefront finite support. In [13], we have shown that the distribution of the background field level remained the same during the wavefront propagation.

Therefore, the SNR will increase until reaching a maximum value of 18 dB just before the impact on the EUT of the wavefront, as σ does not change. This SNR parameter, γ, has been originally introduced in [14] to quantify the quality of a reconstructed signal on a point-like transceiver by considering the ratio between the squared level of the peak of s(t), $I_{peak} = s^2(0)$, and the level of the noise, I_{noise}, defined as the square of s(t) rms value computed apart from the coherent portion of the reconstructed signal time length τ, shown in Figure 3. It has been proven that, for ensemble averages, γ depends on parameters resumed in the equation below and as RCs are ergodic systems, temporal averages are equivalent to spatial ones so $\gamma = \mu^2 / \sigma^2$:

$$\gamma = \frac{\langle s(0) \rangle^2}{\langle s^2(t) \rangle} = \frac{\mu^2}{\sigma^2} \cong \frac{4\sqrt{\pi} n_0 \Delta\omega}{1 + 2\pi n_0 / \Delta T} \tag{1}$$

These parameters are: the modal density of the cavity, n_0, considered constant over the bandwidth $\Delta\omega$ of x(t) and the length ΔT of the signal recorded by the TRM during the first step of time reversal. We must remind that the converging cylindrical wavefront is propagating in the free-space conditions during the temporal windows just before focusing towards the EUT. Thus, we verified that the magnitude of the field is proportional to the reciprocal of the attenuation level $1/\sqrt{r}$ for a divergent cylindrical wave, at least for a distance r from the phase center greater than the far-field distance criteria. Therefore, the SNR when the wavefront focuses into an electrically small EUT will be higher than for a large one as it is closer to its phase center. An interesting idea can be to design the equivalent array of the TREC system to shift the center of phase to be tangential to the EUT and thus ensure the maximum SNR with respect to equation (1).

V. IMPACT OF THE TRM ANTENNAS ON THE WAVEFRONT QUALITY

In order to estimate the number of antennas needed for the TRM and their influence on the wavefront quality, we analyze the distribution of the field magnitudes over one circle as we did previously. This time, we represent in the Figure 7 the frequency of occurrence of the field values for 2,4,6 and 8 TRM antennas used simultaneously in the TREC system.

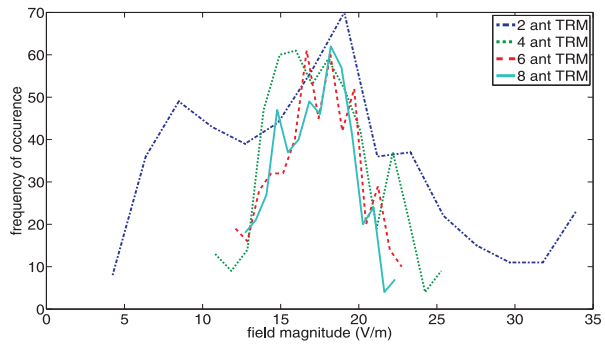

Figure 7. Frequency of occurrence of the field magnitudes for different numbers of active TRM antennas.

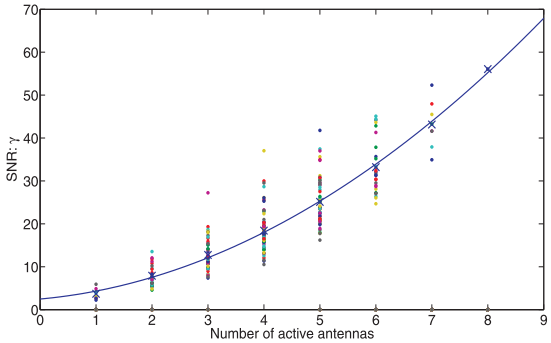

Figure 8. Dispersion of the SNR for a number of simultaneous active TRM antennas from 1 to 8. The quadratic line is the curve fitting mean values (represented by crosses) of the SNR for each case.

We can observe that from 2 to 4 antennas the rms standard deviation decreases rapidly (6.8 V/m to 4 V/m) while from 6 to 8 it is less visible (3.4 V/m to 2.7 V/m). We normalized the field magnitudes to the number of used antennas in order to have the same average value for the different cases. Still, we are interested in the impact of the TRM antennas positions on the SNR. For that purpose, we have computed γ corresponding

to the combinations of each active antenna set. For example, there are 8 combinations with only one active antenna whereas 70 possibilities exist with 4 of them. We can see on Figure 8 the spread of the SNR value for the different configurations of active TRM antennas. The highest rms standard deviation is 6.3 for the case of 6 active antennas. This is because the position of the antenna will allow coupling more or less energy to the cavity resonant modes. We can notice than the solid quadratic curve is fitting the means values of the SNRs.

VI. CONCLUSION AND PERSPECTIVES

We have demonstrated in this paper the feasibility of high-intensity, coherent, and deterministic cylindrical wavefronts generation inside an RC. We have shown that the time-reversal technique must be adapted to enable EMI shielding tests, as EUT are generally electrically large systems leading to the development of a new testing tool: the TREC system.

A study on the influence of the TRM antennas number on the quality of the reconstructed wavefront is carried out through numerical simulations. We saw that this quality increases quadratically with respect to the number of used TRM antennas but shows dispersion depending on the positions of the active TRM antenna sets.

The TREC system is potentially able to generate any waveform that is already possible to radiate with the equivalent array in free space. Therefore, we propose in [14] a procedure to generate directive wavefronts inside the TREC to be able to do a real-time sweeping of deterministic wave incoming directions on the EUT just by changing the signals on the TRM antennas.

Finally, in order to propose the TREC system as a complementary EMC tool with respect to ACs and RCs, we will extend the properties of the TREC to generate polarized deterministic wavefront. To achieve that aim, a completely new challenge will be to validate these concepts in a fully 3D structure and compare the numerical results to experimental setups.

REFERENCES

[1] S. Yang, K. Lozano, A. Lomeli, H. D.. Foltz, R. Jones, "Electromagnetic interference shielding effectiveness of carbon nanofiber/LCP composites," *Composites Part A, Elsevier*, 2005

[2] D. D. L. Chung, "Materials for Electromagnetic Interference Shielding," *Journal of Materials Engineering and Performance*, Springer, 2000

[3] "Radiated, Radio-Frequency, Electromagnetic Field Immunity Test," *International Standard, Standard IEC61000-4-3*, 1995.

[4] M. L. Crawford, G. H. Koepke, "Design, evaluation and use of a reverberation chamber for performing electromagnetic susceptibility/vulnerability measurements," *NBS Tech.*, vol. Note 1092, no. 4, 1986.

[5] M. Bäckström, J. Loren, O. Lunden, L. Jansson, "Directional Properties of Microwave Coupling for Apertures and Shielded Equipment Measured in Mode-Stirred and Anechoic Chambers," *NIST April 28- May 2*, 1997.

[6] M. Fink, "Time reversal of ultrasonic Fields: part I. Basic principles," *IEEE Trans. Ultrason. Ferro-electr. Freq. Control*, vol. 39, no. 5, pp. 555-566, Sept. 1992.

[7] N. Chakroun, M. Fink, F. Wu, "Application of the time reversal to the non destructive monitoring," *Journal de physique*, Vol. 4(2), no. 5, 1994.

[8] H. Tortel, G. Micolau, M. Saillard, "Decomposition of the Time Reversal Operator for Electromagnetic Scattering," *Journal of Electromagnetic Waves and Applications*, Volume 13, Number 5, 1999, pp. 687-719(33)

[9] G. Lerosey, J. De Rosny, A. Tourin, M. Fink, "Focusing beyond the diffraction limit with far-field time reversal," *Science*, Vol. 315, no5815, pp. 1120-1122, 2007.

[10] G. Lerosey, J. de Rosny, A. Tourin, A. Derode, G. Montaldo, M. Fink, "Time Reversal of Electromagnetic Waves," *American Physical Society, Phys. Rev. Lett.*, vol. 90, no. 19, pp. 193904, May 2004.

[11] A. E. H. Love, "The Integration of Equations of Propagation of Electric Waves," *Phil Trans. Roy Soc. London*, Ser. A, 197, pp. 1-45, 1901.

[12] H.Weyl, "Uber das Spektrum der Hohlraumstrahlung," *Z. Reine Angew. Math.*, vol. 141, pp. 163–181, 1912.

[13] H. Moussa, A. Cozza, M. Cauterman, "Directive Wavefronts Inside a Time Reversal Electromagnetic Chamber," *submitted to EMC2009 IEEE Symposium*, Aug. 2009.

[14] J. de Rosny, "Milieux réverbérants et réversibilité," *PhD thesis*, Université Paris VI - Pierre et Marie Curie, Oct. 2000.